

OPTIMIZATION OF FIRST PASSAGE TIMES BY MULTIPLE COOPERATING MOBILE TRAPS

A. E. LINDSAY*, J. C. TZOU†, AND T. KOLOKOLNIKOV‡

Abstract. We study the mean capture time of an unbiased random walker by multiple absorbing mobile traps in bounded domains of one and two spatial dimensions. In one dimension, we consider multiple traps undergoing prescribed oscillatory motion on an interval with reflecting or absorbing boundary conditions. We develop trap co-operation strategies which optimize the mean capture time. We find that as the frequency of oscillation passes through certain fixed values, the optimal trap strategy alternates between oscillating exactly in phase and exactly out-of-phase with neighboring traps. We also demonstrate a scenario in which the optimal configuration is neither in phase nor antiphase. In two dimensions, we consider two small traps rotating with the same angular velocity ω inside a unit disk, and characterize the optimal positions (radii of rotation and relative phase) of the two traps as a function of ω and trap radius $\varepsilon \ll 1$. We identify several distinguished regimes in ω where the optimal configuration can be distinctly characterized. In particular, in the $\omega \sim \mathcal{O}(1)$ regime, the optimal configuration jumps from one in which two traps rotate antipodal and along the same radius to one where the two traps rotate on the same side of the disk but at different radii. In addition, we demonstrate an algebraic approach to obtaining optimal configurations of N rotating traps as $\omega \rightarrow \infty$.

Key words. mean first passage time, multiple mobile traps, trap cooperation, asymptotic analysis, optimization strategy.

AMS subject classifications. 35B25, 35C20, 35J05, 35J08.

1 Introduction

We study the problem for the mean first passage time (MFPT) of a randomly diffusing particle to multiple absorbing mobile traps which undertake a prescribed motion in bounded regions of one and two spatial dimensions. Random motion is a ubiquitous transport mechanism in many biological, physical and chemical systems. Often, a significant event is triggered when a dispersing particle reaches a particular site, or meets another particle. Consequently, many important processes may be formulated as a MFPT problem for the expected time taken for a particle to hit a trap. One dimensional examples include the financial scenario where an investor sells a stock when it reaches a certain threshold, and stochastic neuronal membrane activity in which spiking activity is triggered when an action potential threshold is reached [2, 17].

In two and three dimensions, a special case known as a *narrow escape* or *narrow capture problem* (see, e.g., [3, 9, 23, 29, 32–34]) arises when the size of the trap is small in comparison to that of the search domain. For example, intra-cellular processes require proteins to diffuse in the cytoplasm until they reach the nucleus where they are transported to the interior through nuclear pore complexes distributed on its surface [13, 14, 16, 25]. The cell nucleus is modeled as a small interior trap as its volume is small in comparison to that of the whole cell. Conversely, when ions diffuse in search of an open ion channel located on the cell membrane [7, 19, 29, 32], the traps may be modeled as small absorbing portions of an otherwise reflective boundary. The search for antigen presenting molecules in lymph node tissue by T cells may be modeled as a three dimensional narrow escape problem with interior traps [12] in which MFPT yields insight into immune system recognition. In ecological examples, the duration of a predator’s search for prey and the distance it covers factor into its chances of survival. The prey, such as herds of buffalo or deer, may be modeled as small stationary patches [24, 26] and the predator assumed to undergo either a pure random search or a random search with centralizing tendency toward a den site [22, 27, 28, 35]. The applications of narrow escape problems are numerous, and we refer to [8, 20, 21] for detailed reviews.

Existing mathematical treatments of these examples predominately assume that traps occupy a fixed location over time. However, in many applications traps are known to be mobile. In the action potential example cited previously, it has been demonstrated [2, 17] that the threshold for initiation does not remain constant, but changes due to external input as well as from memory effects due to previous spiking events. As such, the stochastically varying membrane potential chases a moving target. The expected time to the next triggering event is then a MFPT problem involving a mobile trap. Similarly, in the example of intra-cellular transport, the cell nucleus is in motion before and after mitosis [36]; therefore proteins must diffuse to mobile targets in order to complete their processes. In ecological problems, prey undergo migration or make journeys in search of food or water and so predators must locate transient targets. In this work, we investigate mean survival times of random walkers in the presence of multiple traps undergoing prescribed motion along a constrained path. In particular, we study the question of how multiple mobile searchers

*Department of Applied & Computational Mathematics & Statistics, University of Notre Dame, Notre Dame, IN, 46556, USA. (a.lindsay@nd.edu)

†Mathematics Department, University of British Columbia, Vancouver, BC, V6T 1Z2, Canada. (tzou.justin@gmail.com)

‡Department of Mathematics and Statistics, Dalhousie University, Halifax, NS, B3H 3J5, Canada. (tkolokol@gmail.com)

should cooperate in order to most quickly locate a diffusing target. We cite as a typical scenario the search of a lost person by a team of rescuers.

MFPT problems involving mobile traps have been gaining attention for their various applications and also because there is not yet a systematic methodology for their analysis as exists for stationary traps. A recent review on MFPT problems in bounded domains [4] cited the generalization to mobile traps as an interesting extension. Many works in this new direction have focused on one dimensional problems, where the mobile trap undergoes either random motion or advances in one direction linearly in time [5, 6, 11, 15, 18, 37].

An overarching question is whether a mobile trap is more or less effective than a stationary one. In [39], it was shown that a single trap undergoing sinusoidal motion in a bounded one-dimensional interval is more effective only when the frequency exceeds a certain threshold. This criticality can be heuristically understood from a balance between two competing factors that contribute to the MFPT. First, the placement of the absorbing trap at the center of the one-dimensional interval results in a lower MFPT. Second, trap mobility allows a trap to explore its space more effectively and so improves its trapping ability. Therefore, a mobile trap is superior to a stationary one only when it moves quickly enough to overcome the detrimental effects of moving away from optimal spatial locations.

A similar two dimensional result was established in [38] for a single trap rotating inside the unit disk. The presence of two variables of motion (frequency and radius of rotation) poses a simple optimization problem: for a given frequency, what is the radius of rotation that would minimize average mean first passage times? In this setting, a similar criticality is observed where the trap must rotate sufficiently quickly to offset the detrimental effect of moving off the origin - the optimal spatial location for the unit disk [23].

In the present work, we analyze MFPT problems in bounded one and two dimensional regions with *multiple* mobile traps with prescribed trajectories and emphasize the optimization of average (or global) MFPT with respect to the relative motion between the traps. In §2, we consider a diffusing particle on a one-dimensional interval with reflecting or absorbing end points and absorbing internal traps with small amplitude oscillations at common frequency ω and centered on fixed points with separation ℓ . A schematic of the one dimensional two trap problem is displayed in Fig. 1.1(a). The linearity of the governing equations allows for trivial extension of the present work to trap trajectories with multiple frequency components. However, we focus herein on trajectories described by a single frequency component as the resulting motion minimizes the MFPT under a fixed kinetic energy constraint.

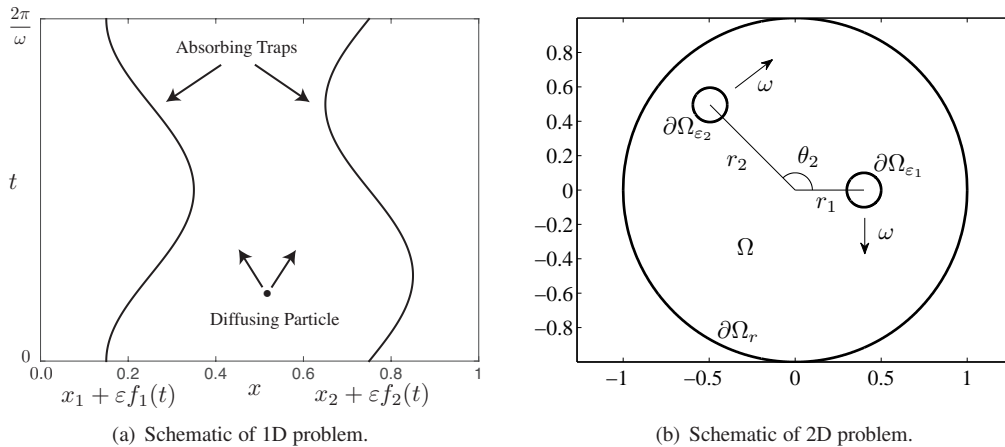


Figure 1.1: (a) A schematic of the 1D problem with two traps. Two traps oscillate in time at the same frequency tracing out the paths indicated by the curves. Their relative phase is arbitrary. (b) A schematic of the problem 2D problem with two traps. In the reference frame rotating clockwise at frequency ω , the first trap is placed on the horizontal axis (without loss of generality) at a distance r_1 from the origin. The second trap is phase shifted counterclockwise by angle θ_2 and is a distance r_2 from the origin. Both traps have common radius ε .

We show in the one dimensional setup of Fig. 1.1(a) that the mean capture time of the particle averaged uniformly over all starting locations (often referred to as global MFPT) is minimized when the two traps oscillate either exactly

in phase or exactly antiphase, depending on the sign a certain quantity $\chi(\omega\ell^2)$ where

$$\chi(z) = \left[\frac{\cosh \sqrt{\frac{z}{2}} \sin \sqrt{\frac{z}{2}} + \sinh \sqrt{\frac{z}{2}} \cos \sqrt{\frac{z}{2}}}{\cos \sqrt{2z} - \cosh \sqrt{2z}} \right],$$

the trap separation as $\varepsilon \rightarrow 0$ is ℓ and the common frequency is ω . The oscillatory nature of $\chi(z)$ means that the optimal strategy alternates as the frequency of the trap's motion increases. In §2.1, these results are extended to N traps oscillating about fixed points x_j with small amplitude ε and common frequency ω . We determine that the globally optimal cooperation strategy corresponds to neighboring traps oscillating either exactly in phase or exactly out-of-phase depending on the sign of $\chi(\omega\ell_j^2)$ where $\ell_j = x_{j+1} - x_j$. We also illustrate a scenario in which the optimizing strategy does not necessarily correspond to being exactly in or out-of-phase with adjacent traps.

In §3, we consider N small traps of radius $0 < \varepsilon \ll 1$ rotating clockwise with common frequency ω at distances r_j from the center of a unit disk with $j = 1, \dots, N$ (schematic in Fig. 1.1(b)). We use a matched asymptotics approach (e.g., [23, 29, 38]) to compute the global MFPT of a randomly diffusing particle. Our formulation allows for arbitrary phase differences between the traps. For $N = 2$, we perform a numerical optimization of the global MFPT with respect to the two radii of rotation in addition to the relative phase. The results of optimization show that as ω increases past a critical $\mathcal{O}(1)$ frequency, the optimal configuration of the traps switches from rotating at the same radius but π -radians out of phase to rotating at different radii but exactly in phase. We also show that in the regime $\mathcal{O}(1) \ll \omega \ll \mathcal{O}(\varepsilon^{-1})$, the optimal radii of N traps divides the unit disk into N annuli of equal area (with the outermost radius approaching the boundary). We also derive an analogous result in the regime $\omega \gg \mathcal{O}(\varepsilon^{-1})$. We further use a hybrid numeric-asymptotic method [10, 38] to interpolate between these two regimes, showing that the transition between the regimes is smooth. In §4, we draw conclusions and list open avenues for further work. For a related problem involving optimizing the fundamental Neumann eigenvalue on a two-dimensional domain with N small Dirichlet holes, see [23] and the references therein.

2 Multiple Traps in 1D

In this section we consider the MFPT problem in a bounded one dimensional interval with reflecting stationary endpoints and two mobile internal traps undergoing prescribed motion. The approach is readily applicable to non-stationary or absorbing boundaries. The formulation of this problem leads to the partial differential equation [6, 31, 39]

$$u_t + u_{xx} + 1 = 0; \quad 0 < x < 1; \quad 0 < t < \frac{2\pi}{\omega}; \quad (2.1a)$$

$$u_x(0, t) = u_x(1, t) = 0, \quad u(x, 0) = u\left(x, \frac{2\pi}{\omega}\right), \quad (2.1b)$$

together with the trapping conditions

$$u(x_1 + \varepsilon f_1(t)) = u(x_2 + \varepsilon f_2(t)) = 0. \quad (2.1c)$$

For convenience, the diffusivity has been normalized to one. The traps are moving with a common frequency, but with a phase shift according to their cooperation strategy,

$$f_1(t) = \sin \omega t, \quad f_2(t) = \sin \omega(t - \phi), \quad \phi \in \left(0, \frac{2\pi}{\omega}\right). \quad (2.1d)$$

The goal is to calculate the global MFPT

$$\tau(\phi; \omega) = \frac{\omega}{2\pi} \int_0^{\frac{2\pi}{\omega}} \int_{x=0}^1 u(x, t) dx dt, \quad (2.2)$$

which gives a measure of the trapping effectiveness of the configuration. From this quantity, optimizing configurations of ϕ and ω can be determined. In the limit $\varepsilon \rightarrow 0$, (2.1) admits a regular expansion of form

$$u(x, t) = u_0(x) + \varepsilon u_1(x, t) + \varepsilon^2 u_2(x, t) + \mathcal{O}(\varepsilon^3), \quad (2.3a)$$

with $u_x(0, t) = u_x(1, t) = 0$. Expanding around the trapping boundaries supplements the equations with the internal conditions

$$u_0(x_j) = 0, \quad u_1(x_j) = -u'_0(x_j)f_1, \quad u_2(x_j) = -\frac{u''_0(x_j)}{2}f_1^2 - u'_1(x_j)f_1, \quad j = 1, 2. \quad (2.3b)$$

This subdivides the interval $\Omega = [0, 1]$ into three distinct regions

$$\mathcal{R}_1(t) = (0, x_1 + \varepsilon f_1(t)), \quad \mathcal{R}_2(t) = (x_1 + \varepsilon f_1(t), x_2 + \varepsilon f_2(t)), \quad \mathcal{R}_3(t) = (x_2 + \varepsilon f_2(t), 1). \quad (2.3c)$$

Order ε^0 : The problem for the leading order solution $u_0(x, t)$ is

$$u_{0t} + u_{0xx} + 1 = 0; \quad -1 < x < 1; \quad u_{0x}(0) = u_{0x}(1) = 0, \quad u(x_j) = 0, \quad j = 1, 2, \quad (2.4)$$

which has solution

$$u_0(x) = \frac{1}{2} \begin{cases} -x^2 + x_1^2, & x \in \mathcal{R}_1(t); \\ -x^2 + (x_1 + x_2)x - x_0x_1, & x \in \mathcal{R}_2(t); \\ (x_2 - x)(x_2 + x - 2), & x \in \mathcal{R}_3(t). \end{cases} \quad (2.5)$$

Order ε^1 : In region \mathcal{R}_1 , the boundary conditions are $u_{1x}(0) = 0$ together with

$$u_1(x_1) = -u'_0(x_1)f_1 = \frac{x_1}{2i} \left(e^{\omega_+^2 t} - e^{\omega_-^2 t} \right), \quad (2.6)$$

which gives rise to a correction equation featuring the operator

$$\phi_{xx} + \phi_t = 0, \quad \phi(x, 0) = \phi\left(x, \frac{2\pi}{\omega}\right). \quad (2.7a)$$

The general solution of (2.7a) which matches the boundary conditions (2.6) is

$$\phi(x, t; \omega) = e^{\omega_-^2 t} [A_1 \cosh \omega_+ x + B_1 \sinh \omega_+ x] + e^{\omega_+^2 t} [A_2 \cosh \omega_- x + B_2 \sinh \omega_- x], \quad \omega_{\pm} = \sqrt{\pm i \omega}, \quad (2.7b)$$

for constants A_1, A_2, B_1, B_2 . It is convenient to work with a complex form of the solution until the final result, at which point the real form is obtained. Fitting the relevant boundary conditions for $u_1(x_j)$ at $j = 1, 2$, gives the solutions in each region to be

$$u_1 = \frac{x_1}{2i} \left(e^{i\omega t} \frac{\cosh \omega_- x}{\cosh \omega_- x_1} - e^{-i\omega t} \frac{\cosh \omega_+ x}{\cosh \omega_+ x_1} \right), \quad x \in \mathcal{R}_1; \quad (2.8a)$$

$$u_1 = \frac{\ell}{4i} \left(\frac{e^{\omega_+^2 t}}{\sinh \omega_- \ell} \left[\frac{\sinh \omega_- (x - x_2) + \sinh \omega_- (x_2 - x_1)}{e^{\omega_-^2 \phi} \sinh \omega_- (x - x_1)} \right] - \frac{e^{\omega_-^2 t}}{\sinh \omega_+ \ell} \left[\frac{\sinh \omega_+ (x - x_2) + \sinh \omega_+ (x_2 - x_1)}{e^{\omega_+^2 \phi} \sinh \omega_+ (x - x_1)} \right] \right), \quad x \in \mathcal{R}_2; \quad (2.8b)$$

$$u_1 = \frac{x_2 - 1}{2i} \left(e^{\omega_+^2 t} \frac{\cosh \omega_- (x - 1)}{\cosh \omega_- (x_2 - 1)} e^{\omega_-^2 \phi} - e^{\omega_-^2 t} \frac{\cosh \omega_+ (x - 1)}{\cosh \omega_+ (x_2 - 1)} e^{\omega_+^2 \phi} \right), \quad x \in \mathcal{R}_3, \quad (2.8c)$$

where $\ell = x_2 - x_1$. As $u_1(x, t)$ has zero mean over $t \in (0, \frac{2\pi}{\omega})$, it does not make a direct contribution to τ in (2.2). However, $u_{1x}(x_j)$ for $j = 1, 2$ contributes to τ through the boundary conditions on $u_2(x_j)$ given in (2.3b).

Order ε^2 : Taking the general form $u_{1x}(x_j) = a_j e^{\omega_-^2 t} + b_j e^{\omega_+^2 t}$ where a_j and b_j are coefficients taken from (2.8), the boundary conditions on $u_2(x_j)$ from (2.3b) are

$$u_2(x_j) = -\frac{u''_0(x_j)}{2}f_1^2 - u'_1(x_j)f_1 = \frac{1}{2} - \frac{a_j}{2i} + \frac{b_j}{2i} + \mathcal{O}(e^{2\omega_{\pm}^2 t}).$$

The general solution is therefore of form $u_2(x, t) = u_{2h}(x) + u_{2p}(x, t)$ where $u_{2p}(x, t)$ is the periodic component

with zero mean over $t \in (0, \frac{2\pi}{\omega})$ and makes no contribution to the value of τ . Therefore only $u_{2h}(x)$ is required in each of the sub regions. As u_{2h} satisfies a homogeneous Neumann condition in regions $\mathcal{R}_1, \mathcal{R}_3$, its value is constant in those regions while in \mathcal{R}_2 , Dirichlet conditions are applied at either end of the region resulting in a linear form for u_{2h} :

$$u_{2h} = \frac{1}{2} - \frac{x_1}{4} (\omega_+ \tanh \omega_+ x_1 + \omega_- \tanh \omega_- x_1), \quad x \in \mathcal{R}_1 \quad (2.9a)$$

$$u_{2h} = \frac{(x - x_1)}{4} \left[\frac{\omega_+}{\sinh \omega_+ \ell} - \frac{\omega_-}{\sinh \omega_- \ell} \right] \sin \omega \phi + \frac{1}{4} - \frac{\ell}{8} \left[\frac{\omega_+}{\sinh \omega_+ \ell} \begin{pmatrix} \cosh \omega_+ \ell \\ +e^{i\omega \phi} \end{pmatrix} + \frac{\omega_-}{\sinh \omega_- \ell} \begin{pmatrix} \cosh \omega_- \ell \\ +e^{-i\omega \phi} \end{pmatrix} \right], \quad x \in \mathcal{R}_2 \quad (2.9b)$$

$$u_{2h} = \frac{1}{2} - \frac{1 - x_2}{4} (\omega_+ \tanh \omega_+ (1 - x_2) + \omega_- \tanh \omega_- (1 - x_2)), \quad x \in \mathcal{R}_3. \quad (2.9c)$$

The value of τ is calculated by integration in each subregion with application of Leibniz's rule. This gives

$$\tau = \frac{\omega}{2\pi} \int_0^{\frac{2\pi}{\omega}} \left[\int_{\mathcal{R}_1} u dx + \int_{\mathcal{R}_2} u dx + \int_{\mathcal{R}_3} u dx \right] dt = \tau_0 + \varepsilon^2 \tau_2 + \dots, \quad (2.10)$$

where, after much algebra and simplification of complex valued expressions,

$$\begin{aligned} \tau_0 &= \frac{x_1^2}{3} + \frac{(1 - x_2)^3}{3} + \frac{\ell^3}{12}; \\ \tau_2 &= -\frac{\sqrt{2\omega} x_1^2}{4} \left(\frac{\sin \sqrt{2\omega} x_1 + \sinh \sqrt{2\omega} x_1}{\cos \sqrt{2\omega} x_1 + \sinh \sqrt{2\omega} x_1} \right) - \frac{\sqrt{2\omega} (1 - x_2)^2}{4} \left(\frac{\sin \sqrt{2\omega} (1 - x_2) + \sinh \sqrt{2\omega} (1 - x_2)}{\cos \sqrt{2\omega} (1 - x_2) + \sinh \sqrt{2\omega} (1 - x_2)} \right) \\ &\quad + \frac{\ell}{2} + \frac{\sqrt{2\omega} \ell^2}{8} \left(\frac{\sin \sqrt{2\omega} \ell + \sinh \sqrt{2\omega} \ell}{\cos \sqrt{2\omega} \ell - \cosh \sqrt{2\omega} \ell} + 2 \left[\frac{\cosh \sqrt{\frac{\omega}{2}} \ell \sin \sqrt{\frac{\omega}{2}} \ell + \sinh \sqrt{\frac{\omega}{2}} \ell \cos \sqrt{\frac{\omega}{2}} \ell}{\cos \sqrt{2\omega} \ell - \cosh \sqrt{2\omega} \ell} \right] \cos \omega \phi \right). \end{aligned}$$

The local extrema of $\tau = \tau(\phi)$ are $\omega \phi = 0, \pi$ and correspond to the two traps being exactly in or out phase with each other. The nature of these critical points is determined by

$$\frac{d^2\tau}{d\phi^2} = -\varepsilon^2 \frac{\sqrt{2\omega} \frac{5}{2} \ell^2}{4} \chi(\omega \ell^2) \cos \omega \phi, \quad \chi(z) = \left[\frac{\cosh \sqrt{\frac{z}{2}} \sin \sqrt{\frac{z}{2}} + \sinh \sqrt{\frac{z}{2}} \cos \sqrt{\frac{z}{2}}}{\cos \sqrt{2z} - \cosh \sqrt{2z}} \right]. \quad (2.11)$$

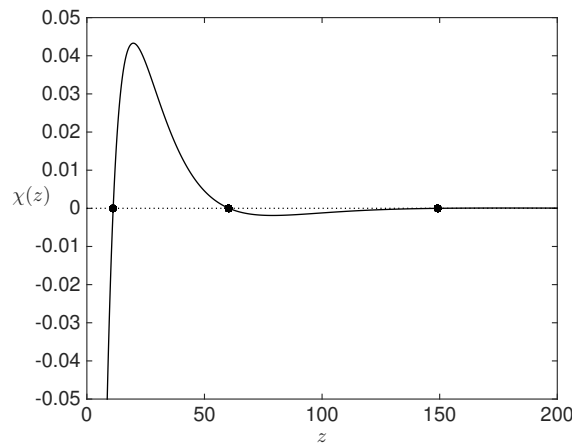


Figure 2.1: Plot of $\chi(z)$ from (2.11) with first three roots indicated.

Therefore, the MFPT is minimized by the traps moving in phase ($\phi = 0$) when $\chi(\omega\ell^2) < 0$ and by out of phase ($\phi = \pi/\omega$) when $\chi(\omega\ell^2) > 0$. The graph of $\chi(z)$ in Fig. 2.1 indicates that its sign changes over certain intervals of $z = \omega\ell^2$. Applying a large argument approximation to $\chi(z_k) = 0$ implies that these thresholds are approximated by

$$z_k \approx \frac{\pi^2}{8}(-1 + 4k)^2, \quad k = 1, 2, 3, \dots, \quad (2.12)$$

which agrees closely with values obtained from numerical solution of $\chi(z_k) = 0$ given in Table 2.1. Therefore, the optimal alignment strategy of the traps alternates as the quantity $\omega\ell^2$ increases.

	z_1	z_2	z_3
Approximate	11.1033	60.4513	149.2778
Numerical	11.1866	60.4517	149.2778

Table 2.1: Approximate (2.12) and numerical values for the critical $z = \omega\ell^2$ over which the optimal cooperation strategy changes.

2.1 N traps in 1D

The analysis of the previous section can easily be extended to accommodate N traps undergoing motion with relative phases to one another. The 1D domain (x_1, x_N) is expressed as union of $N - 1$ intervals $\cup_{j=1}^{N-1} \mathcal{R}_j(t)$ where

$$\mathcal{R}_j(t) = (x_j + \varepsilon f_j(t), x_{j+1} + \varepsilon f_{j+1}(t)), \quad f_j(t) = \sin \omega(t - \phi_j), \quad \ell_j = x_{j+1} - x_j.$$

In this case all traps, including the end points, are absorbing and we assume the cooperation phases ϕ_j are free variables over which to optimize. Following the same process as the two trap problem yields that

$$\tau \sim \sum_{j=1}^{N-1} \frac{\ell_j^3}{12} + \varepsilon^2 \sum_{j=1}^{N-1} \left[\frac{\ell_j}{2} + \frac{\sqrt{2\omega}\ell_j^2}{8} \left(\frac{\sin \sqrt{2\omega}\ell_j + \sinh \sqrt{2\omega}\ell_j}{\cos \sqrt{2\omega}\ell_j - \cosh \sqrt{2\omega}\ell_j} + 2\chi(\omega\ell_j^2) \cos \omega(\phi_{j+1} - \phi_j) \right) \right]. \quad (2.13)$$

where $\ell_j = x_{j+1} - x_j$. When the intervals have common length, $\ell_j = \ell$ for $j = 1, \dots, N - 1$, the conclusions are the same as the two trap case, i.e. the MFPT is minimized by moving in phase with the neighboring trap if $\chi(\omega\ell^2) < 0$ and out of phase with neighboring traps if $\chi(\omega\ell^2) > 0$. For non uniform spacing, finding the lowest MFPT is reduces to minimizing $f(s_1, \dots, s_n) = \sum_{j=1}^n a_j \cos s_j$ for $s_j \in (0, 2\pi)$. The global minimum of this function is $-\sum_{j=1}^n |a_j|$ which is attained when $s_j = 0$ if $a_j < 0$ and $s_j = \pi$ if $a_j > 0$. Consequently, the co-operation strategy for N traps to minimize MFPT is

$$\phi_{j+1} - \phi_j = \begin{cases} 0 & \text{if } \chi(\omega\ell_j^2) < 0; \\ \frac{\pi}{\omega} & \text{if } \chi(\omega\ell_j^2) > 0, \end{cases} \quad (2.14)$$

with a corresponding minimum MFPT

$$\tau = \sum_{j=1}^{N-1} \frac{\ell_j^3}{12} + \varepsilon^2 \sum_{j=1}^{N-1} \left[\frac{\ell_j}{2} + \frac{\sqrt{2\omega}\ell_j^2}{8} \left(\frac{\sin \sqrt{2\omega}\ell_j + \sinh \sqrt{2\omega}\ell_j}{\cos \sqrt{2\omega}\ell_j - \cosh \sqrt{2\omega}\ell_j} - 2|\chi(\omega\ell_j^2)| \right) \right]. \quad (2.15)$$

Similarly, the global MFPT τ is maximized by adopting the opposite phase cooperation strategy to (2.14).

2.2 Adaptation to neighboring traps

As a demonstration of this theory in which the optimal strategy is not exactly in phase or antiphase, we suppose a fixed configuration of traps is present with common frequency ω and individual phases. We then insert an additional trap of frequency ω at location x_k with phase ϕ_k . The contribution to the MFPT τ which depends only on the phase

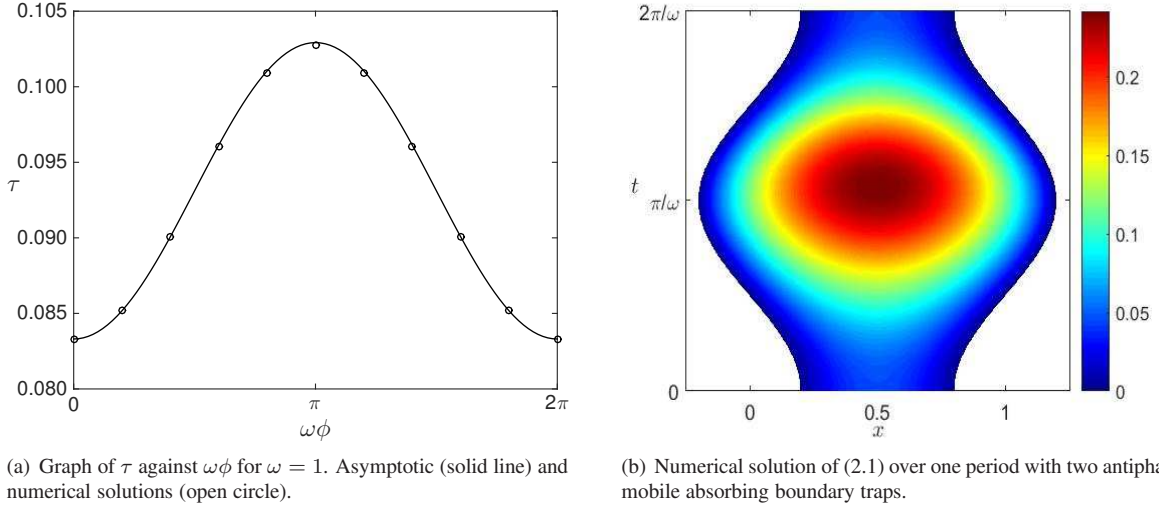


Figure 2.2: Validation of the asymptotic theory with two mobile boundary traps and $\omega = 1$. (a) Agreement of numerical and asymptotic theories as the phase difference between the two traps varies. (b) Numerical computation of the MFPT over one period with two antiphase absorbing mobile boundary traps.

ϕ_k of the additional trap is

$$\mathcal{I}_k = \frac{\varepsilon^2}{\sqrt{8\omega}} [z_k \cos \omega(\phi_{k+1} - \phi_k) + z_{k-1} \cos \omega(\phi_k - \phi_{k-1})], \quad z_k = \omega \ell_k^2 \chi(\omega \ell_k^2),$$

where x_{k+1} and x_{k-1} are the locations of the traps adjacent to the inserted one. Assuming ϕ_{k-1} and ϕ_{k+1} are fixed, the local extrema of this interaction function are the two solutions $\phi_k^\pm \in (0, 2\pi/\omega)$ of the equation

$$\tan \omega \phi_k^\pm = \frac{z_k \sin \omega \phi_{k+1} + z_{k-1} \sin \omega \phi_{k-1}}{z_k \cos \omega \phi_{k+1} + z_{k-1} \cos \omega \phi_{k-1}}. \quad (2.16)$$

Therefore, the optimal interaction strategies are not simply in or out of phase with the adjacent traps, but determined by a weighted average of their phases. The nature of each local extrema follows from the sign of

$$\frac{d^2 \mathcal{I}_k}{d^2 \phi_k}(\phi_k^\pm) = -\omega^2 \mathcal{I}_k(\phi_k^\pm) = -\frac{\varepsilon^2 \omega^{\frac{3}{2}}}{\sqrt{8}} \sec \omega \phi_k^\pm [z_k \cos \omega \phi_{k+1} + z_{k-1} \cos \omega \phi_{k-1}].$$

As an example, consider two mobile traps centered at $x = 0, 1$ with fixed phases $\omega\phi = 0, \frac{\pi}{4}$ respectively and common frequency ω . An additional mobile trap is centered at location $0 < s < 1$ with phase ϕ_s and frequency ω . From (2.16), the optimizing values of ϕ_s satisfy

$$\tan \omega \phi_s^\pm = \frac{(1-s)^2 \chi(\omega(1-s)^2) \sin \frac{\pi}{4}}{(1-s)^2 \chi(\omega(1-s)^2) \cos \frac{\pi}{4} + s^2 \chi(\omega s^2)}. \quad (2.17)$$

In Fig. 2.3, we display the solution of (2.17) for values of $\omega = 5$ and $\omega = 50$. The optimal adaptation strategy is observed to depend quite sensitively on the frequency ω and the spatial placement of the trap.

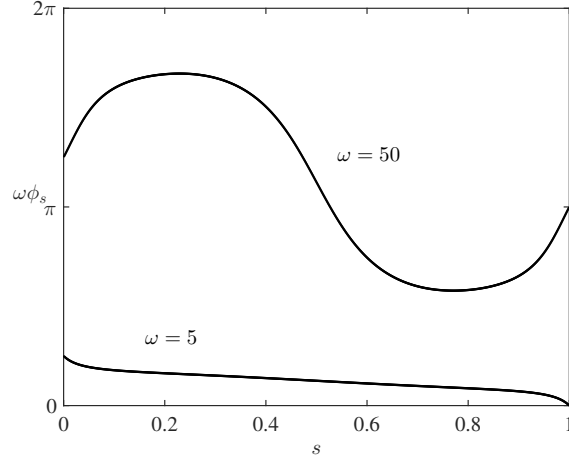


Figure 2.3: The MFPT minimizing phase $\omega\phi_s^-$ of a trap inserted as a function of spatial placement $s \in (0, 1)$ for $\omega = 5$ and $\omega = 50$. Curves obtained from solution of (2.17).

3 N traps on a unit disk

In this section, we seek optimal cooperation strategies for two small identical mobile traps in two dimensions. We formulate the problem for the case of N traps, but perform numerical optimization only for the two trap case. In analogy to the formulation of mobile traps in 1D, the nondimensionalized MFPT u for a Brownian particle in a 2D domain Ω in the presence of a mobile trap undergoing 2π -periodic motion in time satisfies the three dimensional boundary value problem

$$\Delta u + u_z + 1 = 0, \quad \mathbf{x} \in \Omega \setminus \Omega_{\text{trap}}(z), \quad z \in [0, 2\pi), \quad (3.1a)$$

$$u = 0, \quad \mathbf{x} \in \partial\Omega_{\text{trap}}(z), \quad \partial_n u = 0, \quad \mathbf{x} \in \partial\Omega_r, \quad z \in [0, 2\pi), \quad (3.1b)$$

$$u(\mathbf{x}, 0) = u(\mathbf{x}, 2\pi), \quad \mathbf{x} \in \Omega \setminus \Omega_{\text{trap}}(z). \quad (3.1c)$$

In (3.1), Ω_r is the reflective outer boundary of the domain Ω , and $\Omega_{\text{trap}}(z)$ encodes the evolution of the trap's shape and location in time. For the assumption of periodicity, we require $\Omega_{\text{trap}}(z + 2\pi) = \Omega_{\text{trap}}(z)$.

Analysis of (3.1) is in general very difficult. We therefore consider the special case in which the N traps rotate at the same frequency about the center of a unit disk. With this rotational symmetry, the geometry of the corresponding PDE remains two dimensional. A detailed derivation of the PDE for a single rotating trap is given in [38], which we generalize here for N rotating traps. In the frame of N traps each rotating clockwise about the center of the disk with frequency ω , we obtain the mixed Neumann-Dirichlet boundary value problem

$$\Delta u + \omega u_\theta + 1 = 0, \quad \mathbf{x} \in \Omega \setminus \cup_{j=1}^N \Omega_{\varepsilon_j}; \quad (3.2a)$$

$$u = 0, \quad \mathbf{x} \in \partial\Omega_a = \cup_{j=1}^N \partial\Omega_{\varepsilon_j}, \quad j = 1, \dots, N; \quad \partial_n u = 0, \quad \mathbf{x} \in \partial\Omega_r, \quad (3.2b)$$

where u_θ is the derivative of u with respect to the angular coordinate θ . In (3.2), the absorbing set $\partial\Omega_a$ consists of the boundaries of N small traps separated by $\mathcal{O}(1)$ distance, Ω_r the reflective outer boundary of the disk, and $u(\mathbf{x})$ the nondimensional mean first passage time to one of the traps starting from location \mathbf{x} . The j -th trap $\Omega_{\varepsilon_j} = \mathbf{x}_j + \varepsilon\Omega_{0j}$ is centered at location \mathbf{x}_j , where Ω_{0j} is the $\mathcal{O}(1)$ geometry of the trap and ε is its "radius." The schematic and a typical solution (computed using the finite element software FlexPDE [1]) are shown in Figs. 1.1(b) and 3.1, respectively.

Assuming a uniform distribution of starting locations, the average MFPT (or sometimes referred to as global MFPT) is the quantity

$$\bar{u} = \frac{1}{|\Omega|} \int_{\Omega} u(\mathbf{x}) d\Omega, \quad (3.3)$$

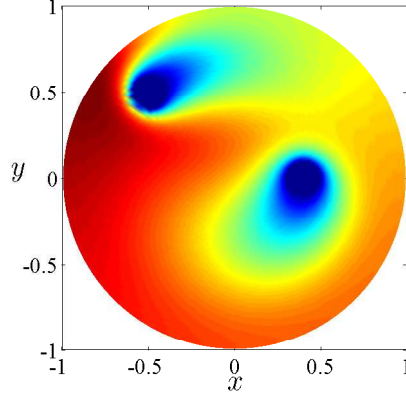


Figure 3.1: A typical 2-trap solution with $\varepsilon = 0.1$, $\omega = 30$, $r_1 = 0.3$, $r_2 = 0.7$, and $\theta_2 = 3\pi/4$. Blue (red) regions indicate small (large) values of u . Notice that MFPT is lower in front of the rotating traps than it is behind. Computed using the finite element software FlexPDE.

where $|\Omega|$ is the size of the domain. Below, we calculate \bar{u} in terms of the trap locations \mathbf{x}_j . We then optimize \bar{u} with respect to the locations. To reduce the number of parameters in the optimization problem, we assume that all traps are circular and share a common radius ε . That is, we assume Ω_{0j} is the unit disk for $j = 1, \dots, N$.

3.1 The regime $\omega \sim \mathcal{O}(1)$

In the regime $\omega \sim \mathcal{O}(1)$, we adopt the method of matched asymptotic expansions [23, 29] to calculate \bar{u} as a function of the relative locations \mathbf{x}_j of N traps. In the inner region near the j -th spike, we let $\mathbf{y} = |\mathbf{x} - \mathbf{x}_j|/\varepsilon$ and $u(\mathbf{x}_j + \varepsilon\mathbf{y}) = U_j(\mathbf{y})$ to obtain the leading order inner problem

$$\Delta U_j = 0, \quad \mathbf{y} \in \mathbb{R}^2 \setminus \Omega_{0j}, \quad U_j \sim S_j \log |\mathbf{y}| - S_j \log d_j \text{ as } |\mathbf{y}| \rightarrow \infty. \quad (3.4)$$

In (3.4), d_j is referred to as the logarithmic capacitance of the j -th trap, which depends on the geometry Ω_{0j} . A list of numerical and analytic values of d for different shapes are given in [30]. For the case we consider, where Ω_{0j} is the unit disk, $d_j = 1$ so that $U_j = S_j \log |\mathbf{y}|$ is the exact solution of (3.4). The quantity S_j , the strength of trap j , is to be determined from a system of linear equations obtained by matching inner and outer solutions. In terms of the outer variables, we calculate the matching condition

$$u \sim S_j \log |\mathbf{x} - \mathbf{x}_j| - S_j \log \varepsilon \text{ as } \mathbf{x} \rightarrow \mathbf{x}_j. \quad (3.5)$$

Since u is logarithmic near each trap, we may express u as a sum of Neumann Green's functions $G(\mathbf{x}, \mathbf{x}_0)$ satisfying

$$\Delta G + \omega G_\theta = \frac{1}{|\Omega|} - \delta(\mathbf{x} - \mathbf{x}_0), \quad \mathbf{x} \in \Omega; \quad (3.6a)$$

$$\partial_n G = 0, \quad \mathbf{x} \in \partial\Omega, \quad \int_\Omega G d\Omega = 0, \quad (3.6b)$$

$$G \sim -\frac{1}{2\pi} \log |\mathbf{x} - \mathbf{x}_0| + R(\mathbf{x}_0, \mathbf{x}_0) \text{ as } \mathbf{x} \rightarrow \mathbf{x}_0. \quad (3.6c)$$

Then in the limit $\varepsilon \rightarrow 0$, we write

$$u = -2\pi \sum_{j=1}^N S_j G(\mathbf{x}, \mathbf{x}_j) + \bar{u}. \quad (3.7)$$

In (3.6c), $R(\mathbf{x}_0, \mathbf{x}_0)$ is the regular part of G as $\mathbf{x} \rightarrow \mathbf{x}_0$, referred to as the self-interaction term. By the integral condition in (3.6b), which uniquely specifies G , \bar{u} in (3.7) is the uniform average of u in (3.3) that we seek to optimize.

To obtain the $N + 1$ equations for S_1, \dots, S_N and \bar{u} , we first compare (3.7) with (3.6) to (3.2) to obtain the solvability condition

$$\sum_{j=1}^N S_j = \frac{1}{2}. \quad (3.8)$$

The other N equations come from applying the matching condition (3.5) at the N trap locations \mathbf{x}_j . Letting $\mathbf{x} \rightarrow \mathbf{x}_i$ in (3.7) and using the limiting behavior of G near \mathbf{x}_i , we calculate

$$-2\pi S_i \left[-\frac{1}{2\pi} \log |\mathbf{x} - \mathbf{x}_i| + R_{ii} \right] - 2\pi \sum_{j \neq i}^N G_{ij} S_j + \bar{u} = S_i \log |\mathbf{x} - \mathbf{x}_i| + \frac{S_i}{\nu}, \quad (3.9)$$

where $R_{ii} \equiv R(\mathbf{x}_i, \mathbf{x}_i)$, $G_{ij} \equiv G(\mathbf{x}_i, \mathbf{x}_j)$, and $\nu \equiv -1/\log \varepsilon \ll 1$. The logarithmic terms in (3.9) match by construction. To write (3.9) in matrix form, we define

$$\mathbf{s} \equiv \begin{pmatrix} S_1 \\ \vdots \\ S_N \end{pmatrix}, \quad \mathbf{e} \equiv \begin{pmatrix} 1 \\ \vdots \\ 1 \end{pmatrix}, \quad \mathcal{E} \equiv \mathbf{e}\mathbf{e}^t, \quad \mathcal{G} \equiv \begin{pmatrix} R_{11} & G_{12} & \cdots & G_{1N} \\ G_{21} & \ddots & \ddots & \vdots \\ \vdots & \ddots & \ddots & G_{N-1,N} \\ G_{N1} & \cdots & G_{N,N-1} & R_{NN} \end{pmatrix}, \quad (3.10)$$

where t denotes the transpose, and \mathcal{G} in (3.10) is the Green's interaction matrix, which encodes information on the locations of the N traps. In contrast to the Green's matrix in [23], \mathcal{G} is not symmetric due to the symmetry-breaking rotation of the traps. We rewrite (3.8) and (3.9) in the form

$$2\pi \mathcal{G}\mathbf{s} + \frac{1}{\nu} \mathcal{I}\mathbf{s} = \bar{u}\mathbf{e}, \quad \mathbf{e}^t \mathbf{s} = \frac{1}{2}, \quad (3.11)$$

where \mathcal{I} is the $N \times N$ identity matrix. Multiplying both sides of (3.11) by \mathbf{e}^t and solving for \bar{u} , we obtain the solution for \bar{u} and the strengths of the traps S_1, \dots, S_N

$$\bar{u} = \frac{1}{N} \left[2\pi \mathbf{e}^t \mathcal{G}\mathbf{s} + \frac{1}{2\nu} \right], \quad \mathbf{s} = \frac{1}{2\nu N} \left[2\pi \left(\mathcal{I} - \frac{1}{N} \mathcal{E} \right) \mathcal{G} + \frac{1}{\nu} \mathcal{I} \right]^{-1} \mathbf{e}. \quad (3.12)$$

We observe in (3.12) that $S_j = (2N)^{-1}$ to leading order in ν^{-1} for all j , and $\bar{u} = (2\nu N)^{-1}$. That is, all traps share a common strength to leading order, and \bar{u} increases logarithmically as $\varepsilon \rightarrow 0$. The effect of trap locations on \bar{u} is therefore a smaller $\mathcal{O}(1)$ correction.

To construct the Green's interaction matrix (3.10) in the case $\omega \neq 0$, we adopt a Fourier series approach where we let $\mathbf{x} = (r \cos \theta, r \sin \theta)$. The Neumann Green's function satisfying (3.6) is then given by [38]

$$G(\mathbf{x}, \mathbf{x}_0; \omega) = G(r, \theta, r_0, \theta_0; \omega) = R_0(r, r_0) + \sum_{m>0} e^{im(\theta-\theta_0)} R_m(r, r_0) + c.c., \quad (3.13a)$$

where the coefficients R_0 and R_m are given by

$$R_0(r, r_0) = \frac{r^2}{4\pi} + \frac{1}{8\pi} [2r_0^2 - 3] - \frac{1}{2\pi} \begin{cases} \log r_0, & 0 < r < r_0 \\ \log r, & r_0 < r < 1 \end{cases}, \quad (3.13b)$$

$$R_m(r, r_0; \omega) = \frac{1}{2\pi} \begin{cases} \left[-\frac{K'_m(c_m)}{I'_m(c_m)} I_m(c_m r_0) + K_m(c_m r_0) \right] I_m(c_m r), & 0 < r < r_0 \\ \left[-\frac{K'_m(c_m)}{I'_m(c_m)} I_m(c_m r) + K_m(c_m r) \right] I_m(c_m r_0), & r_0 < r < 1 \end{cases}, \quad c_m \equiv -i\sqrt{im\omega}. \quad (3.13c)$$

The regular part of G is obtained by using the definition in (3.6c) and expressing $\log |\mathbf{x} - \mathbf{x}_0|$ in terms of its Fourier

series. This calculation yields

$$R(\mathbf{x}_0; \mathbf{x}_0) = \frac{r_0^2}{2\pi} - \frac{3}{8\pi} + \sum_{m>0} \left(R_m(r_0, r_0) - \frac{1}{4\pi m} \right) + c.c. . \quad (3.13d)$$

In (3.13), *c.c.* refers to the complex conjugate of the term involving the summation. In the case where ω , ε are fixed and $N = 2$, we compare in Fig. 3.2 the asymptotic result (3.12) for \bar{u} to full numerical solutions of (3.2) obtained using FlexPDE. In Fig. 3.2(a), we let the polar coordinates of the first trap be $(r_1, \theta_1) = (0.4, 0)$, with the second located at various locations on the ring $r_2 = 0.8$. In Fig. 3.2(b), we fix the angle of the second trap at $\theta_2 = \pi$, and vary r_2 between 0 and 1. In both figures, we observe excellent agreement between the asymptotic formula (3.12) and numerical results.

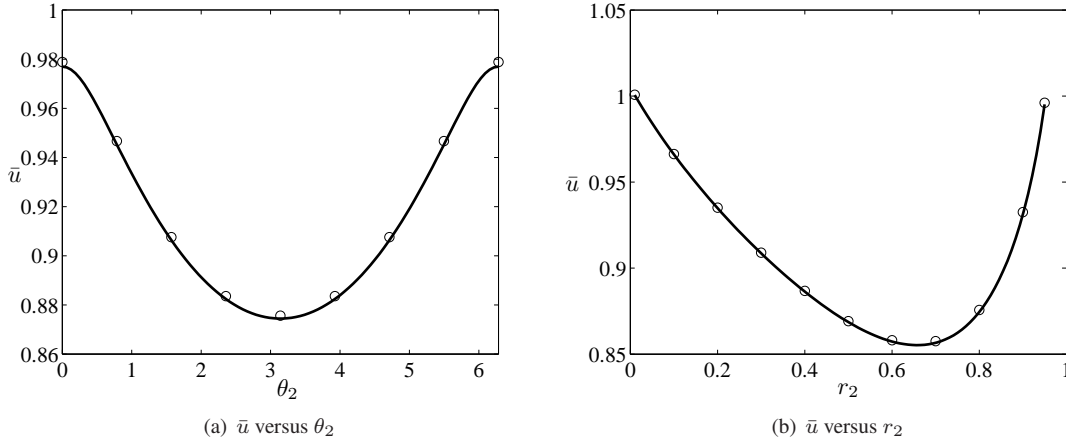


Figure 3.2: Comparison of the asymptotic formula for \bar{u} (3.12) (solid curve) versus numerical results obtained from numerical solution of (3.2) (circles) with parameter values $\omega = 5$ and $\varepsilon = 0.01$. In both figures, the first trap is located at $(r_1, \theta_1) = (0.4, 0)$ while the location of the second (r_2, θ_2) is varied. In (a), $r_2 = 0.8$ while θ_2 is varied. In (b), $\theta_2 = \pi$ while r_2 is varied.

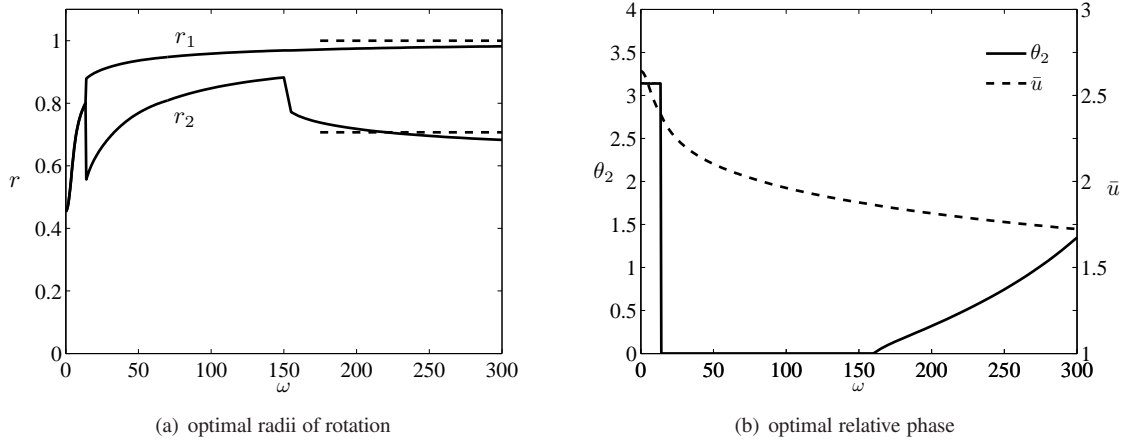


Figure 3.3: Optimal radii of rotation (a) along with relative phase and minimum \bar{u} (b) obtained from optimizing (3.12) for a range of ω . For $\omega \lesssim 14$, the optimal configuration consists of two traps rotating π -phase apart at a common radius. For $14 \lesssim \omega \lesssim 160$, the optimal configuration has the traps rotating exactly in phase but on two different rings. For $\omega \gtrsim 160$, the phase difference becomes nonzero while the traps remain on two different rings. For \bar{u} , its optimal value is decreasing for all ω . The dashed lines in (a) represent the limiting behavior in the subregime $\mathcal{O}(1) \ll \omega \ll \mathcal{O}(\varepsilon^{-1})$.

Using MATLAB's global optimization algorithm `fmincon()`, we optimize \bar{u} in (3.12) over r_1, r_2 , and θ_2 , where, without loss of generality, we set the angular location of one of the traps at $\theta_1 = 0$. The results are shown in Fig. 3.3. For $\omega \lesssim 14$, the optimal configuration consists of two traps rotating π -phase apart at a common radius. For $14 \lesssim \omega \lesssim 160$, the optimal configuration has the traps rotating exactly in phase ($\theta_2 = 0$) but on two different rings. This ‘‘bifurcation’’ is analogous to that found in [38] for one rotating trap, where the optimal radius of rotation is nonzero only when $\omega \gtrsim 3$. The key difference, however, is that since a zero radius of rotation implies that the trap remains stationary, rotation in the one trap case can be *detrimental* to search times when ω is small. That is, one observes a decrease in the optimal MFPT only when $\omega \gtrsim 3$. In contrast, we observe for this two trap configuration that the optimal MFPT is a decreasing function of ω for any ω (dashed curve in Fig. 3.3(b)). For $\omega \gtrsim 160$, the phase difference again becomes nonzero, but the two traps remain on different rings. As we demonstrate in §3.2, the relative phase becomes less important the faster the rotation rate.

We note that, in the small ω limit of Fig. 3.3(a), the result is the same as that obtained from optimizing \bar{u} with the Neumann Green's function and its regular part (3.13) replaced by their $\omega = 0$ variants [23]. For large ω , the optimal radii approach $r_1 = 1/\sqrt{2}$ and $r_2 = 1$, represented by the dashed lines. In this limit, the accuracy of the truncated sum of (3.13d) is diminished due to numerical under- and overflow. In §3.2, we adopt a different approach to calculating \bar{u} in this particular large ω regime that does not involve an infinite sum. We use it to demonstrate the result suggested by the dashed lines in Fig. 3.3(a), and extend it to N traps.

3.2 The sub-regime $\mathcal{O}(1) \ll \omega \ll \mathcal{O}(\varepsilon^{-1})$

In §3.1, optimal configurations could only be found through numerical optimization of a function involving a truncated series. It is thus very difficult to understand how the optimal radii of rotation behave in the limit of large ω . Here, we use a leading order expression for the Neumann Green's function to calculate a closed form expression for the objective function \bar{u} . This simplified result allows the limiting behavior of the optimal radii shown in Fig. 3.3(a) to be calculated explicitly. We note that this is not a distinguished regime, as it is contained within the $\mathcal{O}(1)$ regime. In that sense, we consider ω as being fixed at a very large value while ε is sent to 0. In this limit, a trap rotating on the ring of radius r_0 can be thought of as being almost everywhere on that ring at once. This near-radial symmetry was exploited in [38], where a matched asymptotics approach was employed to compute the leading order radially symmetric solution of (3.6)

$$G(r, r_0) = \frac{r^2 - r_0^2}{4\pi} - \frac{1}{2\pi} \Theta(r - r_0) \log\left(\frac{r}{r_0}\right) + \hat{H}, \quad (3.14a)$$

where $\Theta(z)$ is the Heaviside step function and

$$\hat{H}(r_0) = -\frac{1}{\pi} \left[-\frac{r_0^2}{2} + \frac{3}{8} + \frac{1}{2} \log r_0 \right] + \mathcal{O}(\omega^{-1}). \quad (3.14b)$$

From a separately constructed inner solution, the limiting behavior of G

$$G(r, r_0) \sim \frac{1}{2\pi} \left[-\log |\mathbf{x} - \mathbf{x}_0| - \log\left(\frac{r_0 \omega}{4}\right) - \gamma \right] + \hat{H}, \quad \text{as } \mathbf{x} \rightarrow \mathbf{x}_0, \quad (3.15)$$

yields the leading order regular part of G

$$R(r_0) = \frac{1}{2\pi} \left[-\log\left(\frac{r_0 \omega}{4}\right) - \gamma \right] + \hat{H}(r_0). \quad (3.16)$$

In (3.15), γ is Euler's constant. Recalling that $\mathbf{s} = (2N)^{-1} \mathbf{e}$ to leading order in ν , we calculate the simplified leading order formula for \bar{u}

$$\bar{u} = \frac{\pi}{N^2} \sum_{ij} \mathcal{G}_{ij} + \frac{1}{2\nu N}, \quad (3.17)$$

where \mathcal{G}_{ij} is the ij -th entry of the matrix \mathcal{G} defined in (3.10). For $N = 2$, assuming $r_1 < r_2$, we use (3.14) to calculate

$$\bar{u} = \frac{1}{8} \left[\log\left(\frac{16}{\omega^2}\right) - 2\gamma - 3 + 2(r_1^2 + r_2^2) - 2 \log r_1 - 4 \log r_2 \right] + \frac{1}{4\nu}. \quad (3.18)$$

Finding the critical points of (3.18) by solving $\partial_{r_1} \bar{u} = \partial_{r_2} \bar{u} = 0$ leads to two uncoupled equations for r_1 and r_2 . The result is that \bar{u} is minimized to leading order when r_1 and r_2 are given by

$$r_1 \sim \frac{1}{\sqrt{2}}, \quad r_2 \sim 1, \quad \text{as } \omega \rightarrow \infty \text{ with } \omega \ll \mathcal{O}(\varepsilon^{-1}). \quad (3.19)$$

We make three remarks. The first is that result (3.19) is rather counterintuitive given the suboptimal nature of search locations near boundaries. However, it was shown also [38] in the same subregime $\mathcal{O}(1) \ll \omega \ll \mathcal{O}(\varepsilon^{-1})$ that a single rotating trap is best placed asymptotically close to the boundary of the unit disk. Second, in assuming radial symmetry in constructing G in (3.15), we have lost resolution on θ_2 , the relative phase between the two traps. Because the radial symmetry of u increases with increasing ω , the effect of relative phase diminishes in this regime. Lastly, the two rings of rotation divide the unit disk into two regions of equal area. In fact, it can be easily shown using (3.17) that the optimal radii of rotation for N traps are

$$r_j = \sqrt{\frac{j}{N}}, \quad j = 1, \dots, N. \quad (3.20)$$

The results of [23, 38] show that a single Dirichlet ring on which $u = 0$ is best placed at $r = 1/\sqrt{2}$, which divides the unit disk into two equal areas. In [38], this occurred in the $\omega \rightarrow \infty$ regime with $\omega \gg \mathcal{O}(\varepsilon^{-1})$ regime. The result (3.20), showing that the equal division of area in fact occurs in the $\mathcal{O}(1) \ll \omega \ll \mathcal{O}(\varepsilon^{-1})$ subregime, is thus unexpected. In Fig. 3.4, with $r_1 = 1/\sqrt{2}$ fixed, we verify the formula (3.18) with full numerical solutions of (3.2) for various r_2 . We observe that \bar{u} is minimized very near $r_2 = 1$, consistent with (3.19). The circles (stars) are for $\theta_2 = 0$ ($\theta_2 = \pi$), their similarity showing that the relative phase of the traps has little effect on \bar{u} . We also remark that, in contrast to the case of N optimally placed stationary traps, which share a few concentric rings, (3.20) shows that for sufficiently high rotation frequencies, each trap occupies its *own* ring.

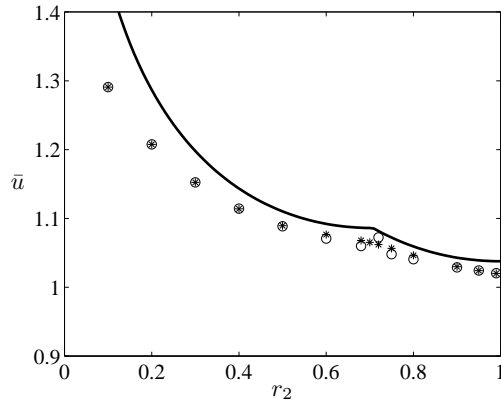


Figure 3.4: Comparison in the regime $\mathcal{O}(1) \ll \omega \ll \mathcal{O}(\varepsilon^{-1})$ of \bar{u} from (3.18) (solid) with that from full numerical solutions of (3.2) (circles and stars). One radius of rotation is fixed at $r_1 = 1/\sqrt{2}$, while the second (r_2) is varied. We observe that \bar{u} is minimized very near $r_2 = 1$, consistent with (3.19). Here, $\omega = 500$ and $\varepsilon = 1 \times 10^{-4}$. The circles (stars) are for $\theta_2 = 0$ ($\theta_2 = \pi$), showing that the relative phase of the traps has little effect on \bar{u} .

3.3 The regime $\omega \sim \mathcal{O}(\varepsilon^{-1})$

In the distinguished regime $\omega = \varepsilon^{-1}\omega_0$ with $\omega_0 = \mathcal{O}(1)$, the equation in the $\mathcal{O}(\varepsilon)$ j -th inner region is no longer the radially symmetric Laplace's equation outside the unit disk. Indeed, with scaling $\mathbf{y} = \varepsilon^{-1}(\mathbf{x} - \mathbf{x}_j)$, both the Δu and $\omega \partial_\theta u$ terms in (3.2) become $\mathcal{O}(\varepsilon^{-2})$. Recalling that the relative phases of the traps has little effect on \bar{u} , we assume for simplicity that they are all located on $\theta_j = 0$. With $U_j(\mathbf{y}) = u(\mathbf{x}_j + \varepsilon \mathbf{y})$, the equation in the j -th inner

region then becomes

$$\Delta U_j + \omega_0 r_j \frac{\partial}{\partial y_2} U_j = 0, \quad |\mathbf{y}| > 1, \quad U_j = 0, \quad |\mathbf{y}| = 1, \quad U_j \sim u_j(\omega_0 r_j) \text{ as } |\mathbf{y}| \rightarrow \infty; \quad \mathbf{y} = (y_1, y_2), \quad (3.21a)$$

where $u_j(\omega_0 r_j)$ is a constant to be found. This inner solution and the outer solution is mediated through an intermediate parabolic layer with scaling $\hat{r} = \sqrt{\omega_0}(r - r_j)/\sqrt{\varepsilon}$ and $\hat{\theta} = 2\pi - \theta$, forming an $\mathcal{O}(\sqrt{\varepsilon})$ layer around the ring $r = r_j$. In this layer, $u = \hat{u}_j$ satisfies the parabolic equation

$$\hat{u}_{j\hat{r}\hat{r}} - \hat{u}_{j\hat{\theta}} = 0, \quad \hat{u}_j(\hat{r}, 0) = \sqrt{\varepsilon} c_j \delta(\hat{r}) + u_j, \quad (3.21b)$$

where c_j is an $\mathcal{O}(1)$ constant. The solution of (3.21b) decays to the constant u_j as $\hat{r} \rightarrow \infty$ so that u in the outer region is approximately constant on the ring $r = r_j$. Therefore, the leading order radially symmetric outer solution satisfies the ODE

$$u_{rr} + \frac{1}{r} u_r + 1 = 0, \quad u = u_j(\omega_0 r_j), \quad r = r_j, \quad u'(0) = u'(1) = 0. \quad (3.21c)$$

The solution to (3.21) was found in [38] for a single rotating trap using a hybrid numeric-asymptotic technique similar to that employed in [10]. Here, we extend the method to the case of two traps, noting that extension to N traps follows in the same manner. Our goal is to calculate u_j in order to uniquely specify the outer equation (3.21c).

We begin by letting $U_j = u_j(\mu_j + 1)$. Substituting into (3.21a), we obtain for μ_j

$$\Delta \mu_j + q_j \frac{\partial \mu_j}{\partial y_2} = 0, \quad |\mathbf{y}| > 1, \quad \mu_j = -1, \quad |\mathbf{y}| = 1, \quad \mu_j \sim 0 \text{ as } |\mathbf{y}| \rightarrow \infty; \quad q_j \equiv \omega_0 r_j. \quad (3.22)$$

The quantity we seek is the flux of μ_j on the boundary of the unit disk Ω_0 ,

$$\Phi_j \equiv \int_{\partial\Omega_0} \frac{\partial \mu_j}{\partial n} dS, \quad (3.23)$$

where $\partial/\partial n$ denotes the outward normal derivative on Ω_0 . The flux may be extracted numerically as follows [10, 38]. We first consider the adjoint Green's function satisfying

$$\Delta \tilde{G} - q_j \frac{\partial \tilde{G}}{\partial \xi_2} = \delta(\boldsymbol{\xi} - \mathbf{z}), \quad \tilde{G} \rightarrow 0 \text{ as } |\boldsymbol{\xi}| \rightarrow \infty, \quad (3.24)$$

which may be solved to give

$$\tilde{G}(\boldsymbol{\xi}; \mathbf{z}) = -\frac{1}{2\pi} e^{\frac{q_j}{2}(\eta - z_2)} K_0\left(\frac{q_j}{2}|\boldsymbol{\xi} - \mathbf{z}|\right); \quad \boldsymbol{\xi} = (\xi_1, \xi_2), \quad \mathbf{z} = (z_1, z_2). \quad (3.25)$$

In polar coordinates $(\xi_1, \xi_2) \rightarrow (\tilde{r} \cos \tilde{\theta}, \tilde{r} \sin \tilde{\theta})$ and $(z_1, z_2) \rightarrow (\rho \cos \phi, \rho \sin \phi)$, the solution to (3.22) can then be expressed in terms of \tilde{G} in (3.25) as

$$\mu_j(\rho \cos \phi, \rho \sin \phi) = \int_0^{2\pi} \frac{\partial \tilde{G}}{\partial \tilde{r}} \Big|_{\tilde{r}=1} d\tilde{\theta} + \int_0^{2\pi} \left(\tilde{G} \frac{\partial \mu_j}{\partial \tilde{r}} \right) \Big|_{\tilde{r}=1} d\tilde{\theta} - q_j \int_0^{2\pi} \tilde{G} \Big|_{\tilde{r}=1} \sin \tilde{\theta} d\tilde{\theta}. \quad (3.26)$$

Note that all integrals in (3.26) are over the boundary of the unit disk $\partial\Omega_0$. To extract the flux $\partial \mu_j / \partial \tilde{r}|_{\tilde{r}=1}$, we impose the boundary condition $\mu_j = -1$ on $\rho = 1$, yielding

$$-\int_0^{2\pi} \tilde{G} \Big|_{\tilde{r}=\rho=1} \frac{\partial \mu_j}{\partial \tilde{r}} \Big|_{\tilde{r}=1} d\tilde{\theta} = \frac{1}{2} + \int_0^{2\pi} \frac{\partial \tilde{G}}{\partial \tilde{r}} \Big|_{\tilde{r}=\rho=1} d\tilde{\theta} - s_0 \int_0^{2\pi} \tilde{G} \Big|_{\tilde{r}=\rho=1} \sin \tilde{\theta} d\tilde{\theta}. \quad (3.27)$$

The integral equation (3.27) may then be solved numerically for $\partial \mu_j / \partial \tilde{r}|_{\tilde{r}=1}$. In (3.27), the $1/2$ term is a result of evaluating μ_j on $\partial\Omega_0$ and thus integrating over only half of the delta function in its Green's function representation.

To express Φ_j in terms of the flux f_j of u , we recall that $u \sim u_j(\mu_j + 1)$ near $\mathbf{x} = \mathbf{x}_j$. Substituting into (3.23), we obtain

$$u_j = \frac{f_j}{\int_{\partial\Omega_0} \frac{\partial\mu_j}{\partial n} dS} = -\frac{f_j}{\pi} \frac{-\pi}{\int_{\partial\Omega_0} \frac{\partial\mu_j}{\partial n} dS}. \quad (3.28)$$

where f_j is the flux of u on the j -th trap. We rewrite (3.28) as

$$u_j = -\frac{f_j}{\pi} u_{0j}, \quad u_{0j} \equiv \frac{-\pi}{\Phi_j}, \quad (3.29)$$

where Φ_j is defined in (3.23). The quantity $u_{0j}(q_j)$, whose dependence on $q_j \equiv \omega_0 r_j$ is through that of μ_j , was computed in [38] and reproduced in Fig. 3.5. To find u_j in (3.29), we require N equations for f_j . We demonstrate this

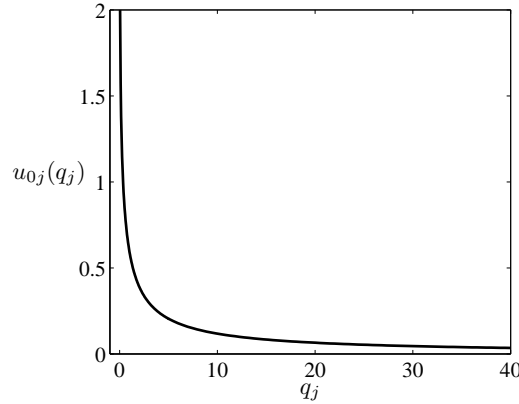


Figure 3.5: Plot of u_{0j} versus $q_j \equiv \omega_0 r_j$.

for two traps. In the three distinct regions, we compute u_r as

$$u_r = -\frac{r}{2} + \begin{cases} 0, & 0 < r < r_1; \\ \frac{2c}{r}, & r_1 < r < r_2; \\ 1, & r_2 < r < 1, \end{cases} \quad c \equiv \frac{1}{\log \frac{r_1}{r_2}} \left[u_1 - u_2 + \frac{1}{4} (r_1^2 - r_2^2) \right]. \quad (3.30)$$

The total fluxes on the rings $r = r_1$ and $r = r_2$ must, respectively, be f_1 and f_2 . We calculate that

$$f_1 = -2\pi c, \quad f_2 = 2\pi c - \pi. \quad (3.31)$$

We remark that $f_1 + f_2 = -\pi$, as expected from applying the divergence theorem to (3.2). Finally, with c defined in (3.30), we obtain u_1 and u_2

$$u_1 = \frac{1}{2} \frac{u_{01}(r_1^2 - r_2^2 - 4u_{02})}{\log \frac{r_1}{r_2} - 2u_{01} - 2u_{02}}, \quad u_2 = \frac{1}{2} \frac{u_{02} \left(2 \log \frac{r_1}{r_2} - r_2^2 + r_1^2 - 4u_{01} \right)}{\log \frac{r_1}{r_2} - 2u_{01} - 2u_{02}}, \quad r_1 < r_2. \quad (3.32)$$

The mean of u is then obtained from computing the mean of the solution of (3.21c), which yields

$$\bar{u} = \frac{1}{8 \log \frac{r_1}{r_2}} \left[(r_2^2 - r_1^2)(r_2^2 - r_1^2 + 4(u_2 - u_1)) + (4r_2^2 + 8u_2 - 3 - 4 \log r_2) \log \frac{r_1}{r_2} \right], \quad r_1 < r_2. \quad (3.33)$$

In Fig. 3.6(a), with $\omega_0 = 10$, $\varepsilon = 0.001$ and $r_2 = 0.95$, we compare (3.33) (solid) with full numerical solutions of (3.2) (circles) for a range of r_1 . We observe good agreement not only in the value of \bar{u} , but in where the minimum

occurs. Further confirmation of the analysis (not shown) comes from the agreement of u_1 and u_2 given asymptotically by (3.32) with that obtained from numerical solutions of (3.2). In Fig. 3.6(b), we show the optimal radii of rotation obtained from optimizing (3.33) with respect to r_1 and r_2 .

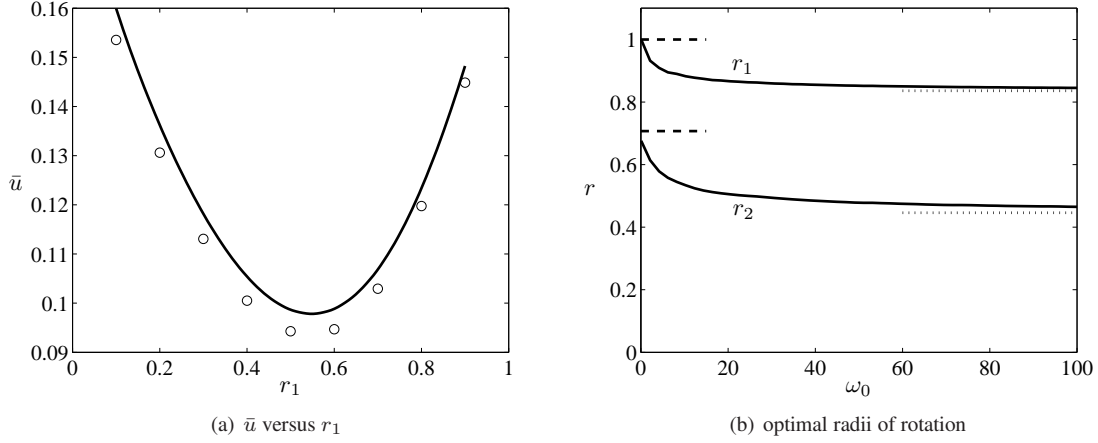


Figure 3.6: In (a), with $\omega_0 = 10$, $\varepsilon = 0.001$, and $r_2 = 0.95$, we compare \bar{u} in (3.33) for a range of r_1 (solid) against full numerical results of (3.2) (circles). The asymptotic result (3.33) correctly predicts the location of the minimum. In (b), we show optimal radii r_1 and r_2 that minimize \bar{u} . The dashed lines are the optimal radii $r_1 = 1/\sqrt{2}$ and $r_2 = 1$ in the limit $\omega_0 \rightarrow 0$. The dotted lines represent the limit in which $\omega_0 \rightarrow \infty$, discussed in §3.4.

We remark that this regime interpolates between the $\mathcal{O}(1) \ll \omega \ll \mathcal{O}(\varepsilon^{-1})$ subregime ($\omega_0 \rightarrow 0$) and the $\omega \rightarrow \infty$ regime with $\omega \gg \mathcal{O}(\varepsilon^{-1})$ ($\omega_0 \rightarrow \infty$). Taking the latter limit in (3.21a), it is simple to see that, since $\partial_{y_2} U_j = 0$ and $U_j = 0$ on $\partial\Omega_0$, we must have $u_j = 0$. This corresponds to the case in which $u = 0$ on the ring $r = r_j$, which occurs in the limit of infinitely fast trap rotation. This limit is discussed in detail in §3.4, the two-trap result of which is represented by the dotted lines in Fig. 3.6(b).

To analyze the former limit $\omega_0 \rightarrow 0$ (dashed lines in Fig. 3.6(b)), we must look at the corresponding limit $q_j \rightarrow 0$ in (3.25) and (3.27). From the asymptotics of modified Bessel functions, we calculate the leading order behavior of \tilde{G} and $\partial_{\tilde{r}} \tilde{G}|_{\tilde{r}=\rho=1}$

$$\tilde{G} \sim \frac{1}{2\pi} [\log q_j + \log |\boldsymbol{\xi} - \mathbf{z}| - \log 4 + \gamma] + \mathcal{O}(q_j \log q_j), \quad \left. \frac{\partial \tilde{G}}{\partial \tilde{r}} \right|_{\tilde{r}=\rho=1} \sim \frac{1}{4\pi} + \mathcal{O}(q_j), \quad \text{as } q_j \rightarrow 0, \quad (3.34)$$

where γ is Euler's constant. With (3.34) in (3.27), we have to leading order that

$$-\frac{1}{2\pi} [\log q_j - \log 4 + \gamma] \int_0^{2\pi} \left. \frac{\partial \mu_j}{\partial \tilde{r}} \right|_{\tilde{r}=1} d\tilde{\theta} - \frac{1}{4\pi} \int_0^{2\pi} \log [(\cos \tilde{\theta} - \cos \phi)^2 + (\sin \tilde{\theta} - \sin \phi)^2] \left. \frac{\partial \mu_j}{\partial \tilde{r}} \right|_{\tilde{r}=1} d\tilde{\theta} = 1. \quad (3.35)$$

Since the limit $\omega_0 \rightarrow 0$ in (3.22) corresponds to μ_j approaching a radially symmetric solution, we assume that $\partial_{\tilde{r}} \mu_j$ is uniform on $\partial\Omega_0$. The second term in (3.35) consequently integrates to zero, leaving

$$\int_0^{2\pi} \left. \frac{\partial \mu_j}{\partial \tilde{r}} \right|_{\tilde{r}=1} d\tilde{\theta} \sim -\frac{2\pi}{\log q_j - \log 4 + \gamma}. \quad (3.36)$$

Using (3.36) in (3.29), and noting that $\partial_n = -\partial_{\tilde{r}}$, we obtain the asymptotic behavior of u_{0j} in the limit of small q_j

$$u_{0j} \sim -\frac{1}{2} [\log q_j - \log 4 + \gamma]. \quad (3.37)$$

With $q_j = \omega_0 r_j$, substituting (3.37) for u_{01} and u_{02} into (3.33) and discarding terms of $\mathcal{O}(1/\log \omega_0)$ results in precisely (3.18). The optimal radii of rotation then, as depicted in Fig. 3.6(b), approach $r_1 = 1/\sqrt{2}$ and $r_2 = 1$

(dashed lines) as $\omega_0 \rightarrow 0$. As such, the transition between the results of the regimes $\mathcal{O}(1) \ll \omega \ll \mathcal{O}(\varepsilon^{-1})$ and $\omega \sim \mathcal{O}(\varepsilon^{-1})$ is smooth.

3.4 The regime $\omega \rightarrow \infty$ with $\omega \gg \mathcal{O}(\varepsilon^{-1})$

In this regime the MFPT u is radially symmetric and satisfies

$$u_{rr} + \frac{1}{r}u_r + 1 = 0, \quad u(r_j) = 0 \text{ and } u'(0) = u'(1) = 0, \quad 0 \leq r_1, \dots, r_N \leq 1. \quad (3.38)$$

The solution to (3.38) can be obtained in piecewise fashion. The optimal radii are then found by optimizing $\int_0^1 u(r)rdr$ with respect to N variables r_1, \dots, r_N .

We now show how this N -dimensional optimization problem can be reduced to a sequence of $N - 1$ algebraic equations whose solution yields the optimal radii. We first define two functions: let $r_2 = F(r_1, r_3)$ be the optimal ring location r_2 for the MFPT problem on an annulus with Dirichlet boundary conditions on $r = r_1$ and r_3 , and with a ring trap at location $r_2 \in (r_1, r_3)$. That is, let

$$r_2 = F(r_1, r_3) = \operatorname{minarg}_{r_2 \in (r_1, r_3)} \int_{r_1}^{r_3} u(r)rdr, \quad (3.39a)$$

where $u(r)$ solves

$$u_{rr} + \frac{1}{r}u_r + 1 = 0, \quad u(r_1) = u(r_2) = u(r_3) = 0. \quad (3.39b)$$

Similarly, let $r_1 = G(r_2)$ be the optimal location of the ring trap of radius r_1 inside a Dirichlet disk of radius r_2 :

$$r_1 = G(r_2) = \operatorname{minarg}_{r_1 \in (0, r_2)} \int_0^{r_2} u(r)rdr, \quad (3.40a)$$

where $u(r)$ solves

$$u_{rr} + \frac{1}{r}u_r + 1 = 0, \quad u(r_1) = u(r_2) = 0, \quad u'(0) = 0. \quad (3.40b)$$

The following are three key observations that allow us to “decouple” the problem.

- **Observation 1:** For an optimal configuration r_1, \dots, r_N which minimizes $\min_{r_1, \dots, r_N} \int_0^1 u(r)rdr$ of problem (3.38), one has that $r_1 = G(r_2)$, $r_2 = F(r_1, r_3)$, $\dots, r_{N-1} = F(r_{N-2}, r_N)$. In other words, r_2 is optimal for the MFPT with Dirichlet boundary conditions of an annulus of radii r_1 and r_3 , and so on.
- **Observation 2:** If $r_2 = F(r_1, r_3)$ then $\frac{r_2}{r_3} = F(\frac{r_1}{r_3}, 1)$ and similarly, $r_1 = G(r_2) \iff \frac{r_1}{r_2} = G(1)$. This is a simple consequence of the geometric invariance under the scaling of space.
- **Observation 3:** Let A_1, \dots, A_{N+1} be the areas of the regions that are obtained by cutting the disk along the radii r_1, \dots, r_N . Then the sum of even areas is equal to the sum of odd areas. We show below that this condition may be written as

$$r_1^2 - r_2^2 + r_3^2 - \dots + (-1)^N r_N^2 - (-1)^N \frac{1}{2} = 0. \quad (3.41)$$

The first two observations yield the following algorithm to compute the optimal radii of rotation r_1, \dots, r_N . First, define:

$$z_i = \frac{r_i}{r_{i+1}}, \quad i = 1, \dots, N - 1. \quad (3.42)$$

Then from Observation 2, we have that z_1 satisfies $z_1 = G(1)$, while z_i for $i > 1$ may be found sequentially by solving $z_2 = F(z_1 z_2, 1)$, $\dots, z_{N-1} = F(z_{N-1} z_N, 1)$. Once we determine z_1, \dots, z_{N-1} , the radii r_1, \dots, r_N are found by simultaneously solving (3.41) and (3.42).

Explicit solutions of (3.39) and (3.40) show, respectively, that z_1 satisfies

$$4 - \frac{z_1^2 - 1}{z_1^2 \ln(z_1)} = 0, \quad (3.43)$$

while z_{i+1} is related to z_i through

$$4 - \frac{z_{i+1}^2 - 1}{z_{i+1}^2 \ln(z_{i+1})} = \frac{z_i^2 - 1}{\ln(z_i)}, \quad i \geq 1. \quad (3.44)$$

Note that the values of z_i are universal and do not depend on N . The first seven values of z_i are approximately:

k	1	2	3	4	5	6	7
z_k	0.533543	0.712445	0.792159	0.837265	0.866283	0.886517	0.901433

To illustrate this method, we consider the case of $N = 3$ rings. Then we have

$$r_1 = z_1 z_2 r_3, \quad r_2 = z_2 r_3, \quad r_3 = \sqrt{\frac{1/2}{(z_1 z_2)^2 - (z_2)^2 + 1}}, \quad (3.45)$$

which yields the optimal radii of rotation for the three traps $r_1 = 0.33679$, $r_2 = 0.63124$, $r_3 = 0.886022$. We observe that these radii satisfy (3.41) of Observation 3, which we show here. First, consider the following problem:

$$r_m = \min_{r_m \in (r_i, r_o)} \arg \int_{r_i}^{r_o} u(r) r dr, \quad (3.46a)$$

where $u(r)$ solves

$$u_{rr} + \frac{1}{r} u_r + 1 = 0, \quad u'(r_i) = u'(r_o) = 0, \quad u(r_m) = 0. \quad (3.46b)$$

For a fixed r_m , $u(r)$ is given by

$$u = \begin{cases} \frac{r_m^2 - r^2}{4} + \frac{r_i^2}{2} \ln(r/r_m), & r_i < r < r_m; \\ \frac{r_m^2 - r^2}{4} + \frac{r_o^2}{2} \ln(r/r_m), & r_m < r < r_o. \end{cases}$$

To find r_m which minimizes (3.46), we compute

$$\frac{\partial}{\partial r_m} \int_{r_i}^{r_o} u(r) r dr = \int_{r_i}^{r_o} \left(\frac{\partial}{\partial r_m} u \right) r dr = \frac{1}{4r_m} (r_m^2 - r_i^2)^2 - \frac{1}{4r_m} (r_m^2 - r_o^2)^2 = 0.$$

It follows that the minimizing r_m satisfies

$$r_m^2 - r_i^2 = r_o^2 - r_m^2. \quad (3.47)$$

We conclude that for the problem (3.46), the optimal r_m divides the annulus into two regions of equal area. Now consider the optimal solution to (3.38). As an example of this theory, the case $N = 3$ is considered and the optimal solution $u(r)$ shown in Fig. 3.7. The solution $u(r)$ is plotted along with the interior maximizers of u by r_{12} and r_{23} and the areas between maxima and zeros of u as shown. By the property (3.47), we have:

$$A_1 = A_{21}, \quad A_{22} = A_{31}, \quad A_{32} = A_4. \quad (3.48)$$

Moreover, we have

$$A_2 = A_{21} + A_{22}, \quad A_3 = A_{31} + A_{32}, \quad (3.49)$$

where A_1, \dots, A_4 are the areas of the regions that are obtained by cutting the disk along the radii r_1, \dots, r_3 . It follows from (3.48) and (3.49) that $A_1 + A_3 = A_2 + A_4$. This is equivalent to (3.45).

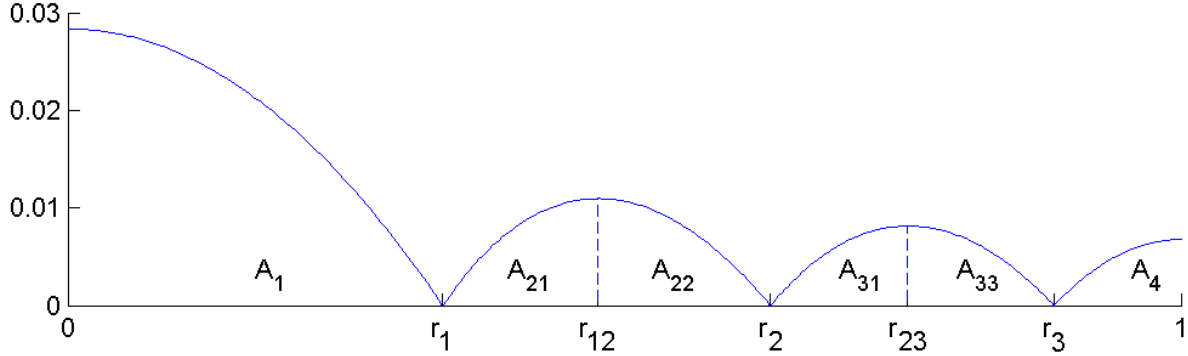


Figure 3.7: Plot of the solution $u(r)$ to (3.38) for $N = 3$ with traps located at the optimal radii.

In Fig. 3.8, we compare the optimal radii in this $\omega \rightarrow \infty$ with $\omega \gg \mathcal{O}(\varepsilon^{-1})$ regime (top row) against those in the $\mathcal{O}(1) \ll \omega \ll \mathcal{O}(\varepsilon^{-1})$ regime (bottom row). In the top row, we observe that as N increases, the outer rings appear to be equally spaced. By contrast, in the bottom row, the rings locations have an explicit formula $r_i = \sqrt{i/N}$ for $i = 1, \dots, N$, and tend to concentrate nearer to the boundary (bottom row).

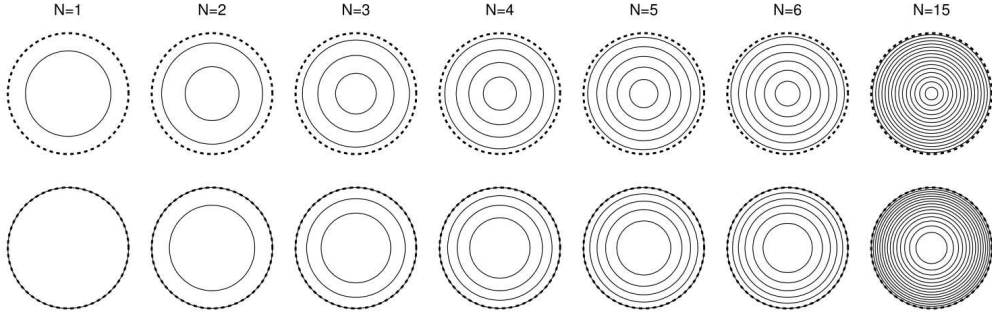


Figure 3.8: Top row: optimal ring positions when $\omega \gg \mathcal{O}(\varepsilon^{-1})$. Bottom row: optimal ring positions when $\mathcal{O}(1) \ll \omega \ll \mathcal{O}(\varepsilon^{-1})$. The ring locations are indicated by solid lines and the boundary $r = 1$ of the disk is denoted by a dashed line. In the bottom row, the outermost ring r_N coincides with the boundary.

4 Discussion

We have used the techniques from [23, 38, 39] to study the MFPT in the presence of multiple mobile traps in one and two dimensions. Very surprising and intricate behaviour is observed even in a one dimensional setting, where we find an infinite sequence of bifurcations (two oscillating traps switch from an in-phase to antiphase configuration infinitely many times) as the oscillation frequency ω is increased. When a trap is forced to adapt to two neighbors whose dynamics are predetermined, its optimal strategy may be neither in-phase nor antiphase with either neighbor.

In two dimensions, the presence of multiple distinguished regimes allows for the characterization of distinct optimal configurations. The simplest of these regimes is $\omega \gg \mathcal{O}(\varepsilon^{-1})$, in which case each rotating trap becomes a Dirichlet ring inside a disk. It is interesting to contrast this to the regime $\mathcal{O}(1) \ll \omega \ll \mathcal{O}(\varepsilon^{-1})$, for which each trap becomes a “ring” but instead of Dirichlet condition on a ring, it is more “porous”, yielding a different radius. For both of these regimes, the relative phase between the two traps is insignificant to leading order, and it is an open question to find the optimal phase. In the $\omega \sim \mathcal{O}(1)$ regime, we observe a bifurcation in which the optimal configuration changes from antiphase rotation with a common radius to an in-phase rotation with different radii.

While our analysis of all regimes is valid for three or more traps, the complexity of the numerical optimizations quickly increases with the number of traps. However, we expect that some behavior observed in the two-trap scenario

would extend to the $N > 2$ case. For example, if three traps rotate slowly, we expect that they rotate with the same radius separated by a $2\pi/3$ phase, and that a similar bifurcation occurs as the rotation rate increases. On the other hand it is unclear what the resulting phase difference (if any) will result on the other side of the bifurcation. For seven or more traps, where the optimal stationary configuration may be a ring of six traps with one at the origin [23], the bifurcation may be more complex.

Our analysis of the two dimensional problem was greatly simplified by the rotational symmetry. It would be very interesting to solve (3.1) either numerically or asymptotically to understand the effects on MFPT of more general trap motion. Within the same rotational framework, one could use (3.1) to investigate whether it is more optimal for two traps to rotate in the same or opposite direction, and whether the result depends on rotation rate in a similar way to what was found in §2 for one dimension.

Another open question is to determine an “optimal” path of the trap. Here, the key issue is to find the right “constraint” on the type of admissible motion. This problem may require an energy constraint, as otherwise one can allow the trap to travel with infinite speed on a space-filling curve. Whether an energy constraint leads to a well-posed optimization problem, and if other or additional constraints may be more appropriate are interesting modeling questions.

The question of proper constraints also arises in the analogous one-dimensional problem, where one seeks an optimal periodic path of $\mathcal{O}(1)$ amplitude. The problem (2.1) for the MFPT would need to be solved numerically for an arbitrary periodic path expressed in terms of Fourier coefficients, which would then be optimized subject to constraints. For example, one may require a fixed energy output over one period, while also penalizing mean square displacement from a certain fixed point.

An overarching theme of this work has been to investigate configurations that result from multiple mobile traps cooperating to optimize a global quantity. It may be interesting to ask what happens when each trap adjusts its motion locally in order to increase its own rate of capturing the Brownian particles, and whether this algorithm leads to any stable configurations.

Acknowledgements

A.E. Lindsay was supported by NSF grant DMS-1516753. J.C. Tzou was supported by a PIMS CRG Fellowship. T. Kolokolnikov was supported by NSERC Discovery Grant No. RGPIN-33798 and NSERC Accelerator Grant No. RGPAS/461907.

References

- [1] FlexPDE is a general-purpose commercial package to solve PDEs, see www.pdesolutions.com.
- [2] Rony Azouz and Charles M Gray. Dynamic spike threshold reveals a mechanism for synaptic coincidence detection in cortical neurons in vivo. *Proceedings of the National Academy of Sciences*, 97(14):8110–8115, 2000.
- [3] O Bénichou and R Voituriez. Narrow-escape time problem: Time needed for a particle to exit a confining domain through a small window. *Physical review letters*, 100(16):168105, 2008.
- [4] O Bénichou and R Voituriez. From first-passage times of random walks in confinement to geometry-controlled kinetics. *Physics Reports*, 539(4):225–284, 2014.
- [5] Alan J Bray and Richard A Blythe. Exact asymptotics for one-dimensional diffusion with mobile traps. *Physical review letters*, 89(15):150601, 2002.
- [6] Alan J Bray and Richard Smith. The survival probability of a diffusing particle constrained by two moving, absorbing boundaries. *Journal of Physics A: Mathematical and Theoretical*, 40(10):F235, 2007.
- [7] Paul C Bressloff and Sean D Lawley. Escape from subcellular domains with randomly switching boundaries. *Multiscale Modeling & Simulation*, 13(4):1420–1445, 2015.
- [8] Paul C Bressloff and Jay M Newby. Stochastic models of intracellular transport. *Reviews of Modern Physics*, 85(1):135, 2013.
- [9] Alexei F Cheviakov, Michael J Ward, and Ronny Straube. An asymptotic analysis of the mean first passage time for narrow escape problems: Part ii: The sphere. *Multiscale Modeling & Simulation*, 8(3):836–870, 2010.
- [10] Jaehyuk Choi, Dionisios Margetis, Todd M Squires, and Martin Z Bazant. Steady advection–diffusion around finite absorbers in two-dimensional potential flows. *Journal of Fluid Mechanics*, 536:155–184, 2005.
- [11] M Chupeau, O Bénichou, and S Redner. Optimal strategy to capture a skittish lamb wandering near a precipice. *arXiv preprint arXiv:1504.05107*, 2015.

- [12] MI Delgado, MJ Ward, and D Coombs. Conditional mean first passage times to small traps in a 3-d domain with a sticky boundary: Applications to T cell searching behaviour in lymph nodes. *Multiscale Modeling & Simulation*, 13(4):1224–1258, 2015.
- [13] Colin Dingwall and Ronald A Laskey. Protein import into the cell nucleus. *Annual review of cell biology*, 2(1):367–390, 1986.
- [14] Carl M Feldherr, Ernst Kallenbach, and Nigel Schultz. Movement of a karyophilic protein through the nuclear pores of oocytes. *The Journal of Cell Biology*, 99(6):2216–2222, 1984.
- [15] Luca Giuggioli, Sebastian Pérez-Becker, and David P Sanders. Encounter times in overlapping domains: Application to epidemic spread in a population of territorial animals. *Physical review letters*, 110(5):058103, 2013.
- [16] Dirk Görlich and Ulrike Kutay. Transport between the cell nucleus and the cytoplasm. *Annual review of cell and developmental biology*, 15(1):607–660, 1999.
- [17] DA Henze and G Buzsaki. Action potential threshold of hippocampal pyramidal cells in vivo is increased by recent spiking activity. *Neuroscience*, 105(1):121–130, 2001.
- [18] D Holcman and I Kupka. The probability of an encounter of two Brownian particles before escape. *Journal of Physics A: Mathematical and Theoretical*, 42(31):315210, 2009.
- [19] D Holcman and Z Schuss. Escape through a small opening: receptor trafficking in a synaptic membrane. *Journal of Statistical Physics*, 117(5-6):975–1014, 2004.
- [20] David Holcman and Zeev Schuss. The narrow escape problem. *SIAM Review*, 56(2):213–257, 2014.
- [21] David Holcman and Zeev Schuss. *Stochastic Narrow Escape in Molecular and Cellular Biology: Analysis and Applications*. Springer, 2015.
- [22] P Holgate. Random walk models for animal behavior. In *International Symposium on Stat Ecol New Haven 1969*, 1971.
- [23] Theodore Kolokolnikov, Michele S Titcombe, and Michael J Ward. Optimizing the fundamental Neumann eigenvalue for the Laplacian in a domain with small traps. *European Journal of Applied Mathematics*, 16(2):161–200, 2005.
- [24] Venu Kurella, Justin C Tzou, Daniel Coombs, and Michael J Ward. Asymptotic analysis of first passage time problems inspired by ecology. *Bulletin of mathematical biology*, 77(1):83–125, 2015.
- [25] AE Lindsay, T Kolokolnikov, and JC Tzou. Narrow escape problem with a mixed trap and the effect of orientation. *Physical Review E*, 91(3):032111, 2015.
- [26] Hannah W McKenzie, Mark A Lewis, and Evelyn H Merrill. First passage time analysis of animal movement and insights into the functional response. *Bulletin of mathematical biology*, 71(1):107–129, 2009.
- [27] L David Mech and Luigi Boitani. *Wolves: behavior, ecology, and conservation*. University of Chicago Press, 2010.
- [28] Akira Okubo and Simon A Levin. The basics of diffusion. In *Diffusion and ecological problems: Modern perspectives*, pages 10–30. Springer, 2001.
- [29] S Pillay, Michael J Ward, A Peirce, and Theodore Kolokolnikov. An asymptotic analysis of the mean first passage time for narrow escape problems: Part I: Two-dimensional domains. *Multiscale Modeling & Simulation*, 8(3):803–835, 2010.
- [30] Thomas Ransford. *Potential theory in the complex plane*, volume 28. Cambridge University Press, 1995.
- [31] Sidney Redner. *A guide to first-passage processes*. Cambridge University Press, 2001.
- [32] Z Schuss, A Singer, and David Holcman. The narrow escape problem for diffusion in cellular microdomains. *Proceedings of the National Academy of Sciences*, 104(41):16098–16103, 2007.
- [33] A Singer, Z Schuss, D Holcman, and RS Eisenberg. Narrow escape, Part I. *Journal of Statistical Physics*, 122(3):437–463, 2006.
- [34] A Singer, Z Schuss, and David Holcman. Narrow escape, Part II: The circular disk. *Journal of statistical physics*, 122(3):465–489, 2006.
- [35] Donald Blair Siniff and CR Jessen. *A simulation model of animal movement patterns*. Academic Press, 1969.
- [36] Paulina J Strzyz, Hyun O Lee, Jaydeep Sidhaye, Isabell P Weber, Louis C Leung, and Caren Norden. Interkinetic nuclear migration is centrosome independent and ensures apical cell division to maintain tissue integrity. *Developmental cell*, 32(2):203–219, 2015.
- [37] Vincent Tejedor, Olivier Bénichou, Ralf Metzler, and Raphael Voituriez. Residual mean first-passage time for jump processes: theory and applications to lévy flights and fractional brownian motion. *Journal of Physics A: Mathematical and Theoretical*, 44(25):255003, 2011.
- [38] Justin C Tzou and Theodore Kolokolnikov. Mean first passage time for a small rotating trap inside a reflective

- disk. *Multiscale Modeling & Simulation*, 13(1):231–255, 2015.
- [39] Justin C Tzou, Shuangquan Xie, and Theodore Kolokolnikov. First-passage times, mobile traps, and hopf bifurcations. *Physical Review E*, 90(6):062138, 2014.